

# STUDIES OF NEUTRINO OSCILLATIONS AT REACTORS

FELIX BOEHM

*Physics Department, California Institute of Technology,  
Pasadena, CA 91125, USA*

E-mail: boehm@caltech.edu

## ABSTRACT

Experiments with reactor neutrinos continue to shed light on our understanding of neutrino oscillations. We review some of the early decisive experiments. We then turn to the recent long baseline oscillation experiments at Palo Verde and Chooz which are leading to the conclusion that the atmospheric neutrino anomaly if attributed to oscillations does not involve an appreciable mixing with the  $\bar{\nu}_e$ . The very long baseline KamLAND experiment is now in the planning stages. Its goal is to help explore the large mixing angle solar solution. A review of the  $\bar{\nu}_e + d$  experiment at Bugey and an outline of the  $\bar{\nu}_e$  magnetic moment studies complete this chapter.

## 1. Introduction

Neutrinos from reactors have played an important and decisive role in the early history of neutrino oscillations<sup>1</sup>. After considerable controversy in the early 1980s, results from the reactors at ILL<sup>2</sup> in 1981, at Goesgen<sup>3</sup> in 1986, and at Bugey<sup>4</sup> in 1995 have found no evidence for neutrino oscillations involving reactor  $\bar{\nu}_e$ . More recently, the Chooz<sup>5</sup> and the Palo Verde<sup>6</sup> experiments have confirmed these findings with greater sensitivity. The purpose of this Chapter is to highlight the developments involving reactor neutrinos and to outline the current status and future studies.

We begin with a brief reminder of the parameters that play a role in neutrino oscillation physics<sup>1</sup>. Assuming, for simplicity, that there are only two neutrino flavors, then the two parameters describing oscillations are the mixing amplitude  $\sin^2 2\theta$  and the mass parameter  $\Delta m^2$ . They are related to the probability of creating a weak interaction state with flavor  $l'$  from a state  $l$  ( $l \neq l'$ ) in an "appearance experiment" through the expression,

$$P_{ll'} = \sin^2 2\theta \sin^2 \frac{1.27 \cdot \Delta m^2 (\text{eV})^2 \cdot L (\text{m})}{E_\nu (\text{MeV})}, \quad (1)$$

$L$  being the distance between neutrino source and detector ("baseline") and  $E_\nu$  the neutrino energy. The probability that a state  $l$  disappears through oscillation is given by  $P_{ll} = 1 - P_{ll'}$ . While reactor  $\bar{\nu}_e$  may oscillate into  $\bar{\nu}_\mu$  or  $\bar{\nu}_\tau$ , these neutrinos cannot be observed via charged current reaction as the energy of the  $\bar{\nu}_e$  at a reactor is insufficient to create a  $\mu$  or a  $\tau$ . A reactor experiment thus explores only the disappearance of the  $\bar{\nu}_e$ .

As the oscillatory function depends on the ratio  $L/E_\nu$ , it can be seen that low

energy reactor neutrinos are well suited in exploring the region of small  $\Delta m^2$  at relatively modest baselines. For example, to explore the parameter  $\Delta m^2$  down to  $10^{-3} eV^2$  a reactor experiment with  $E_\nu$  around 5 MeV requires a baseline of  $L = 1$  km, while an accelerator experiment with  $E_\nu = 5$  GeV would require  $L = 1,000$  km.

It follows from (1) that oscillations manifest themselves through modifications of the energy spectrum of neutrinos arriving in the detector as well as by a change in the total neutrino yield. Both of these aspects can be explored in an experiment.

Reactor experiments with their sensitivity to small  $\Delta m^2$ , have been directed toward exploring the physics of the atmospheric neutrino ratio<sup>7</sup>, a topic described in Chapter 5 of this book. If extended to even larger baselines, these experiments are capable of shedding light on the large mixing angle solar neutrino solution<sup>8</sup>, as discussed in Chapter 4.

Most reactor neutrino detectors are based on the interaction with the proton,

$$\bar{\nu}_e + p = e^+ + n \quad (2)$$

with a threshold of 1.8 MeV. This inverse neutron decay has the largest cross section among neutrino-nuclear reactions. The presence of the time-correlated  $e^+, n$  signature provides a powerful way to retrieve the neutrino signal from the abundant neutron and low energy radioactive backgrounds. A small anisotropy of the reaction products arising from the kinematics of the detection process can be used for "pointing" and thus for background suppression.

## 2. The Reactor Neutrino Spectrum

The neutrino sources for these experiments are large commercial power reactors, each producing about 3GW of thermal power accompanied by neutrino emission at a rate of about  $8 \times 10^{20} \bar{\nu}_e/s$ . As a rule, these reactors run uninterruptedly at full power, except for a refueling cycle of about 1 month per year which provide opportunities for studying the backgrounds of the detector system.

The  $\bar{\nu}_e$  spectrum from a fission reactor and its relation to the reactor's power and status in the burn cycle is well understood today. Pioneering work in deriving this spectrum taking into account the contributions of the fissioning isotopes  $^{235}\text{U}$ ,  $^{239}\text{Pu}$ ,  $^{238}\text{U}$ ,  $^{241}\text{Pu}$ , and  $^{252}\text{Cf}$  and their evolution during the burn cycle has been reported by Vogel<sup>9</sup> in 1981. This extensive modeling work has been supplemented by experimental studies of the electron spectra of the fissioning isotopes  $^{235}\text{U}$ ,  $^{239}\text{Pu}$ , and  $^{241}\text{Pu}$  with an on-line beta spectrometer at ILL Grenoble by Schreckenbach and others<sup>10</sup>. The combined uncertainty for the predicted reactor neutrino spectrum is about 3%.

Figure 1 shows the time evolution of the reactor power associated with the various fissioning fuel components, taken from ref<sup>3</sup>. This information was folded into the

calculated neutrino spectrum <sup>9</sup>.

Fig. 1. Evolution of the contributions to the neutrino spectrum by various reactor fuel components (from ref<sup>3</sup>).

High statistics neutrino experiments involving the total neutrino yields were carried out at the Bugey reactor<sup>11</sup> at short distance from the reactor (where possible oscillation effects are negligible). A 2,000 l water target was installed at a distance of 15 m from one of the 2,800 MW reactors at the Bugey site. As the detector responded to neutrons only it provided an integral cross section of the reaction  $\nu_e + p = e^+ + n$  for neutrinos with energies above the reaction threshold of 1.8 MeV. The event rate was 3,021/d with a background rate (reactor off) of 2,600/d. The cross section, obtained with an absolute accuracy of 1.4%, was compared to the calculated cross section based on V-A theory. Moreover, these results confirm that the reactor neutrino spectrum and its relation to reactor power and fuel composition is well understood. The results are listed in Table 1 together with previous results from Goesgen<sup>3</sup> and Krasnoyarsk<sup>15</sup>. There is an excellent agreement between the measured and calculated neutrino rates for all these experiments.

Table 1: Integral Cross Sections for Reactor Neutrinos on Protons

|                             | Goesgen(86) <sup>3</sup> | Krasnoyarsk(90) <sup>15</sup> | Bugey(94) <sup>11</sup> |
|-----------------------------|--------------------------|-------------------------------|-------------------------|
| $\pm\sigma_{exp}$           | 3%                       | 2.8%                          | 1.4%                    |
| $\sigma_{exp}/\sigma_{V-A}$ | $0.992 \pm 0.04$         | $0.985 \pm 0.04$              | $0.987 \pm 0.03$        |

The parameterization by Vogel and Engel<sup>12</sup> serves as a convenient starting point for present analyses of the measured reactor spectra. As an example, Figure 2 shows the neutrino spectrum from <sup>235</sup>U fission together with the neutrino-proton reaction cross section and reaction yield.

Fig. 2. Energy spectrum, cross section and yield of neutrinos from <sup>235</sup>U fission in a reactor<sup>13</sup>.

### 3. Oscillation Experiments

#### 3.1. The ILL-Grenoble and Goesgen Experiments

Motivated by theoretical developments of neutrino mass and mixing in the 1970s<sup>14</sup> an early reactor experiment was installed at the research reactor of the Laue Langevin

Institute (ILL) in 1977 with the aim of shedding light on oscillations involving  $\bar{\nu}_e$ . The neutrino detector in this ILL experiment<sup>2</sup> consisted of 30 individual cells with liquid scintillator which track the positron, sandwiched between  $^3\text{He}$  proportional chambers to detect the neutron. The distance between reactor and detector was 8.7m. This "disappearance experiment" was searching for a possible reduction of the  $\bar{\nu}_e$  flux as well as for a modification of the energy spectrum observed in the detector. It was found that the measured neutrino spectrum agreed with that calculated<sup>9</sup> and thus revealed no evidence for oscillations down to  $\Delta m^2 = 0.15 \text{ eV}^2$  for  $\sin^2 2\theta \geq 0.25$ .

To enhance the sensitivity of this experiment and to gain information on oscillations with smaller  $\Delta m^2$ , the ILL detector was modified and transferred to the more powerful Goesgen reactor in Switzerland. Three experiments were carried out between 1981 and 1985 with the detector at distances of 37.8 m, 45.9 m, and 64.7 m from the reactor core.

The Goesgen detector<sup>3</sup> consisted of an array of liquid scintillation counters and  $^3\text{He}$  multi-wire proportional chambers, surrounded by an active scintillation veto counter and various shielding, as illustrated in Figure 3.

Fig. 3. The Goesgen neutrino detector (from ref<sup>3</sup>)

The signature of an event is given by a positron pulse in the liquid scintillator followed by a neutron induced reaction in the  $^3\text{He}$  counter. The time correlation and time window chosen are shown in Fig. 4.

Fig. 4. Left: Distribution of time intervals between positron and neutron in Goesgen detector. Right: Pulse shape spectra for reactor-on (solid curve) and reactor-off (dotted curve). The peak to the left represents the neutrino signal (positrons). The right peak is caused by high energy cosmic ray induced neutrons (from ref<sup>3</sup>).

Pulse shape discrimination was instrumental in reducing background events associated with fast neutrons from cosmic rays, as illustrated in Figure 4. No reactor associated backgrounds were seen, as could be verified by comparing backgrounds with reactor-on and reactor-off. The observed correlated positron spectra, corrected for detector response and background, as a function of energy and position, are shown in Figure 5.

Fig. 5. Positron spectra at three positions of the detector (from ref<sup>3</sup>). The solid curves are the predicted positron spectra for no oscillations derived from fitting the reactor neutrino spectra to the data, while the dashed curves are obtained from the calculated neutrino spectra.

In order to compare the spectra taken at various positions and at different times, the relative reactor spectrum for each experiment had to be known. Small differences in reactor fuel composition were taken into account, although these differences were minimized by conducting each experiment over a full fuel cycle. Corrections for the relative difference in fuel composition varied by less than 5%, with a negligibly small uncertainty.

In the data analysis, the experimental positron spectra were compared to calculated spectra in two different ways. First, an analysis (Analysis A) independent of the source neutrino spectrum was conducted. The neutrino spectrum was parameterized and a  $\chi^2$ , calculated for the difference between the experimental yield and the expected yield, was minimized for a fixed set of parameters  $\Delta m^2$  and  $\sin^2 2\theta$ . A maximum likelihood test was used to obtain the exclusion plot shown in Figure 6. In a second analysis (Analysis B) the measured spectra were compared to those calculated<sup>9,10</sup> (also shown in Figure 4) with the results also shown in Figure 6.

Fig. 6. Regions in the parameter space excluded at 90% CL from the Goesgen experiment<sup>3</sup>. Analysis A is based on the ratios of the neutrino spectra at three distances. Analysis B is based on the calculated neutrino spectrum.

It is important to appreciate the sources of the limitations in the accuracy of the mixing angle sensitivity arising from the uncertainties in the absolute normalization of the neutrino spectrum (3%), the detector efficiency calibration using a calibrated neutron source (4%), the reaction cross sections (2%), and the reactor power (2%), compounding to an uncertainty of about 6%.

### 3.2. The Bugey experiments

A high statistics search for neutrino oscillations at the 2,800 MW Bugey reactor with the detectors at 15, 40, and 95m, has been reported by the Bugey group<sup>4</sup> in 1995. In this experiment, three identical 600 l segmented detectors were used. Each detector consisted of 98 prismatic cells viewed by a 3-inch PM on each side. The cells were filled with <sup>6</sup>Li loaded (0.15%) scintillator. Two principal advantages were quoted for the <sup>6</sup>Li loading: the neutron capture time in the scintillator is reduced to 30  $\mu$ s (from about 170 $\mu$ s on protons), and the resulting <sup>3</sup>H and  $\alpha$ -particles can be distinguished from the reaction positrons by pulse shape discrimination. The relative and absolute normalization errors in these experiments were 2% and 5%, respectively. The 95 m experiment provided the most stringent results for the mass parameter  $\Delta m^2$

of  $10^{-2}eV^2$ .

### 3.3. The experiments at Rovno and Krasnoyarsk

We mention briefly the experimental work at the Russian reactors at Rovno<sup>16</sup> and Krasnoyarsk<sup>17</sup>. At the Rovno power reactor a measurement of the total neutrino induced neutron yield was carried out. The detector, at 18m from the reactor, consisted of a water target into which a large number of  $^3\text{He}$  proportional counters were embedded. The observed neutrino yield agreed with that calculated to within about 3%. A similar experiment was carried out at the three-reactor station at Krasnoyarsk. There, the  $^3\text{He}$  neutron counters were embedded in polyethylene and stationed at 57m from reactors 1 and 2, and 231m from reactor 3. While only total yields were obtained, by comparing rates from reactors at different distances, information on oscillations could be derived. These detectors, however, could not provide information on the neutrino spectral shape. Also, these detectors possessed much higher inherent backgrounds than the detectors discussed above which specify the reaction neutron by a  $e^+n$  correlated signal.

### 3.4. The long-baseline experiments at Palo Verde and Chooz

Results from atmospheric neutrino experiments, such as those from Kamiokande<sup>7</sup> have triggered reactor neutrino studies aimed at exploring the parameter region  $\Delta m^2$  between  $10^{-2}$  and  $10^{-3} eV^2$ . Two experiments, both at  $L$  around 1 km, have been conducted recently, one at the French reactor station (2 reactors) at Chooz<sup>5</sup> and the other at the Palo Verde<sup>6</sup> site in Arizona, USA (3 reactors). Both experiments now have results and we describe them below. While these experiments were pursuing their goals, the new Super-Kamiokande<sup>18</sup> results which appeared in 1998 favor the  $\nu_\mu - \nu_\tau$  channel over  $\nu_\mu - \nu_e$  in some regions of the parameter plane.

Another experiment in the Kamioka mine in Japan, referred to as KamLAND<sup>19</sup>, at a much larger distance from a number of power reactors, is still in the proposal stage.

To illustrate the effect from oscillations on the positron spectrum, Fig. 7 shows the expected spectrum for Chooz or Palo Verde for the case of no oscillations as well as for the set of oscillation parameters favored by the Kamiokande results. Clearly, the effects from Kamiokande-type oscillations on the spectrum should be quite pronounced.

Fig. 7. Expected positron spectra for the Chooz or Palo Verde experiments for "no oscillations" and for oscillations given by the Kamiokande parameters.

The Chooz and Palo Verde experiments are based on the reaction  $\bar{\nu}_e + p = e^+ + n$

and rely on a  $(e^+, n)$  correlated signature. Both experiments make use of Gd loaded liquid scintillator. Gd loading reduces the capture time owing to its large thermal neutron capture cross section, and also gives rise to a high energy gamma cascade of up to 8 MeV. Both features are valuable, the short capture time helps reduce random coincidences and the large gamma ray energy allows reduction of backgrounds as the energy threshold can be set above that of radioactive decay products. In both experiments, the amount of Gd dissolved in the scintillator is about 0.1% by weight. At a distance of ca 1 km from the reactor, the detector response is about 5 events per day per ton of scintillator. The Chooz experiment takes advantage of an existing deep tunnel reducing the cosmic ray muon background substantially. The Palo Verde experiment being in a shallow underground laboratory has to cope with a considerably larger muon rate and thus has to rely on powerful background rejection. Because of this, the two detectors are designed quite differently. The Chooz detector consists of a homogeneous central volume of Gd scintillator, while the Palo Verde detector is made from finely segmented detector cells.

#### 3.4.1. The Palo Verde Experiment

The Palo Verde experiment<sup>6</sup> is situated near the Palo Verde nuclear power plant in Arizona (3 reactors, 11 GW thermal power). The detector is installed in an underground cave with 32 mwe overhead at a distance of  $L = 890$  m from reactors 1 and 3, and 750 m from reactor 2. Each reactor is shut down for refueling for a period of ca 40 days every year providing the opportunity for establishing the detector background.

Fig. 8. Schematic view of the Palo Verde detector. One of the cells with PMTs, oil buffers, calibration LEDs and optical fiber flashers is shown lengthwise at the bottom.

Fig. 9. Illustration of the neutrino reaction in the matrix of Gd loaded scintillator.

The detector, shown schematically in Fig. 8, has a fiducial volume of 12 tons. Its liquid scintillator, whose composition is 60% mineral oil, 36% pseudocumene, 4% alcohol, and 0.1% Gd, was developed in collaboration with Bicorn<sup>20</sup>. It has an effective light attenuation length of 10 m for 440 nm light. The detector consists of 66 cells, each 9 m long, of which 7.4 m are active and 0.8 m on each end serve as an oil buffer. There is a 5 inch, low radioactivity photomultiplier attached to each end, allowing both, the anode and the last dynode to be read out. A blue LED installed at 0.9 m from each PM, as well as optical fibers, allow each individual cell to be monitored. A passive water shield, 1 m thick, surrounds the block of active cells to help shield against radioactivity as well as muon induced neutrons. An active veto

counter consisting of 32 12-m long MACRO cells is placed on all 4 long sides while a removable end-veto counter protects the ends of the cell matrix.

A diagram of the detector response showing the  $\bar{\nu}_e$  reaction and the gamma rays from Gd capture is given in Fig. 9.

A neutrino signal consists of a fast (30ns)  $e^+\gamma\gamma$  trigger within a block of 3 x 5 cells, with the first hit having  $E \geq 500\text{keV}$ , and the second hit  $E \geq 30\text{keV}$ . This second hit includes the Compton response from the 511 keV annihilation gammas. This fast triple coincidence is followed by a slow (200  $\mu\text{s}$ ) signal associated with the 8 MeV gamma cascade following neutron capture in Gd within a 5 x 7 scintillator cell matrix.

Energy calibrations could be carried out with the help of small sources that were introduced through a set of Teflon tubes installed alongside a group of detector cells. The response from these sources at various positions made it possible to monitor the attenuation length of the scintillator which exhibited only a negligible decline over the period measured. Fig. 10 shows the light yield along the scintillator cell. The PMT linearity was obtained with the help of a fiber optics flasher while single photo-electron peaks were monitored with a blue LED.

Fig. 10. Light yield along scintillator cell. The attenuation length of the Gd scintillator is 10m.

Inasmuch as the experiment aims at extracting absolute  $\bar{\nu}_e$  induced reaction rates, knowledge of the detection efficiency is essential. The positron efficiency was established with the help of the positron emitter  $^{22}\text{Na}$ . (A calibrated  $^{68}\text{Ge}$  source<sup>21</sup> dissolved in a special cell will also be implemented.) To obtain the neutron efficiency, a calibrated AmBe source was used in a tagged mode, i.e. in coincidence with the 4.4 MeV gamma from  $^{12}\text{C}^*$ . From these calibrations, combined with Monte Carlo simulations an average (over the detector) efficiency was obtained. For the 1999 run this efficiency was found to be 0.112 yielding a neutrino event rate in the detector of  $225 \pm 8$  per day.

From the 1998/99 data, the observed rates for a 147 d run with full reactor power (three reactors on) and a 54.7 d run with reduced power (two reactors on) yielded the positron spectrum shown in Fig. 11. The time structure of the correlated signal is depicted in Fig. 12. The measured decay time of  $35\mu\text{s}$  agrees well with that modeled with a Monte Carlo simulation.

To test the oscillation scenario, a  $\chi$ -squared analysis in the  $(\Delta m^2 - \sin^2 2\theta)$  plane was performed, taking into account the small variations in  $\bar{\nu}_e$  flux from the burn-up dependent fission rate of the reactor. The 90% CL acceptance region was defined according to a procedure suggested by Feldman and Cousins<sup>22</sup>. The data agreed well with the no-oscillation hypothesis. In an independent analysis, which does not rely on the "on" minus "off" scheme, the intrinsic symmetry of the dominant neutron



background with respect to the time sequence of the  $e^+$  and  $n$  signals was implemented to cancel a major part of the neutron induced background. A small neutron background that remained after subtraction of the signal with reversed time sequence was obtained from a Monte Carlo simulation of muon spallation<sup>23</sup>. Experimental data points corresponding to energies  $\geq 10$  MeV (beyond the positron energy spectrum) served to normalize the calculated neutron spectrum. This analysis which was based on subtraction of the neutron background showed no evidence for  $\bar{\nu}_e - \bar{\nu}_X$  oscillations, and thus agreed with the the results of the more traditional "on" minus "off" analysis. The region in the parameter space excluded at 90% CL is depicted by the curve "Palo Verde" in Fig. 16.

Fig. 11. Correlated positron spectrum derived from a 3-reactor run and a 2-reactor run observed and expected for no oscillations.

Fig. 12. Decay time of the fourfold coincidence giving the neutron capture time in our Gd-scintillator.

The segmentation of the Palo Verde detector makes it possible to study the  $\bar{\nu}_e - n$  angular correlation of reaction (2). This, in turn, establishes an independent background determination. From kinematics we find that the neutron moves preferentially in the direction of the incoming neutrino, with an angular distribution limited by

$$\cos(\theta_{\nu,n})_{max} = [2\Delta/E_\nu - (\Delta^2 - m^2)/E_\nu^2]^{1/2}, \quad (3)$$

where  $\Delta = M_n - M_p$ .

From the Monte Carlo simulation it was found that the neutron scattering preserves the angular distribution, resulting in a shift of the mean coordinate of the neutron capture center  $\langle x \rangle = 1.7$  cm<sup>24</sup>. The angular spread after scattering is very pronounced as can be seen in Fig. 13. It should be noted that this effect was first studied by Zacek<sup>25</sup> in connection with the segmented Goesgen detector where the forward/backward ratio was found to be as large as a factor of 2.

Preliminary results<sup>26</sup> give an asymmetry expressed as events in the half plane away from the reactor (forward) minus events in the half plane toward the reactor (backward) of  $109 \pm 44$ , in agreement with a Monte Carlo simulation.

Fig. 13. Angular distribution of scattered (moderated) neutrons with regards to the neutrino direction.

### 3.4.2. The Chooz Experiment

An experiment with a similar aim, however with a substantially different detector was carried out at Chooz by a French-Italian-Russian-US collaboration. This experiment and its results<sup>5</sup>, are reviewed below.

The Chooz detector is comprised of three regions, a central region containing 5 tons of Gd loaded liquid scintillator and surrounded by an acrylic vessel, a containment region with 17 tons of ordinary liquid scintillator, and an outer veto region with 90 tons of scintillator. Fig. 14 shows schematically the arrangement of the Chooz detector.

Fig. 14. Schematic arrangement of the Chooz detector

The inner two regions are viewed by a set of photomultipliers. An independent set of PM detects the light from the veto region. While the positron response is obtained from a signal in the inner region, the neutron response comprises signals from the inner region as well as from the containment region, resulting in a well contained and well resolved Gd capture sum peak at 8 MeV. As mentioned earlier, the Chooz detector is installed in a tunnel, thus reducing the correlated background to less than 10% of the signal.

The data was obtained at various power levels of the two Chooz reactors as these reactors were slowly brought into service. A total of 2991 neutrino events was accumulated in 8209 live hours for reactor-on, and 287 events in 3420 live hours for reactor-off. Normalized to the full power of the two reactors (8.5 GW th) the event rate corresponds to  $27.4 \pm 0.7$  neutrino interactions per day where the error includes contributions from the reaction cross section, the reactor power, the number of protons in the target, and detector efficiency. In comparison, the background rate was  $1.0 \pm 0.1$  per day. The ratio of measured-to-expected neutrino signal is  $1.01 \pm 2.8\%$  (st)  $\pm 2.7\%$  (sys). The total efficiency of the detector was found to be  $69.8 \pm 1.1\%$ .

The positron energy spectrum for reactor-on and reactor-off is shown in Fig. 15, together with a plot of the ratio of measured-to-calculated spectrum.

The neutron capture event characterized by an 8 MeV gamma peak was localized to within  $\sigma_x = 17.4$  cm. The energy resolution for the 8 MeV peak was  $\sigma_e = 0.5$  MeV, or about 1 MeV fwhm. Calibrations for energy, neutron efficiency, and timing, respectively, were carried out with sources of  $^{60}\text{Co}$ ,  $^{252}\text{Cf}$ , and AmBe. The lifetime for neutron capture in the Gd scintillator was found to be  $30.5 \mu\text{s}$ . The combined systematic error was 2.8%.

Figure 16 depicts the Chooz excluded area. Clearly, the Kamiokande region is excluded with a high confidence level, implying the absence of  $\nu_e \leftrightarrow \nu_\mu$  oscillations. The mixing angle limit for large  $\Delta m^2$  from this analysis is  $\sin^2 2\theta < 0.1$  at 90% CL, again based on the widely accepted method by Feldman and Cousins<sup>22</sup>. The 90% limit for  $\Delta m^2$  for maximum mixing from this experiment is  $0.7 \times 10^{-3} eV^2$ .

Fig. 15. Positron energy spectra from the Chooz experiment.

The Chooz collaboration has also compared the spectrum from reactor 2 which is at  $L = 998$  m to that of reactor 1 at  $L = 1115$  m. The relative spectra from the two reactors at different distances provided information on oscillations independent of the absolute yields as described above in the context of the "analysis A" of the Goesgen experiment. For the Chooz experiment, that analysis leads to an exclusion plot consistent with, however less stringent than, that of their analysis involving absolute neutrino yields.

The Chooz analysis also includes a discussion<sup>28</sup> of the neutron angular distribution as mentioned in the section above on Palo Verde.

The parameter space that could be excluded by each of the aforementioned experiments is summarized in Figure 16. The curves are labeled by the experiment and date providing a historical account of the impressive gain in sensitivity over time.

Fig. 16. An overview showing the evolution in time of the 90% excluded regions for the experiments reviewed in this paper. The Kamiokande allowed regions<sup>7</sup> and the region allowed by the recent Super-Kamiokande<sup>18</sup> results if analyzed in the  $\Delta m^2$  vs.  $\Theta_{1,3}$ <sup>27</sup> are also shown by the hatched areas.

### 3.5. The KamLAND Experiment

The KamLAND<sup>19</sup> experiment will be the ultimate long baseline reactor experiment, destined to explore  $\bar{\nu}_e$  disappearance at very small  $\Delta m^2$ . It will be sensitive to exploring the large mixing angle solar MSW solution. The experiment will also address the small mixing angle solar MSW at low neutrino energy by observing the  $\nu_e$  - electron scattering, as well as, by invoking seasonal variations, the vacuum oscillation solution.

The neutrinos originate from 16 nuclear power plants (130 GW thermal power) at distances between 80 and 800 km from the KamLAND detector, with 90% of the neutrino flux produced at sites between 80 and 214 km. The detector will be a 1 kT liquid scintillator to be installed in the former Kamiokande cavity at a depth of 1,000 mwe. The spherical 1 kT scintillator and a surrounding 2.5 m mineral oil shielding are

contained in an 18 m diameter stainless steel sphere that also supports the 2000 17-inch and 20-inch photomultipliers providing a 30% light coverage. The detector light yield is projected to be 100 photoelectrons per MeV. A water volume surrounding the sphere serves as a Cerenkov veto counter. A schematic view of the detector is given in Figure 17. The expected event rate associated with all power plants (51 reactors) is projected to be 750/y. The background rates due to radioactivity and neutrons from muon spallation were obtained from simulations and are predicted to be about 37/y. Under these conditions, a contour plot can be constructed for a 3-year exposure which covers the large mixing angle solar MSW solution, as shown in Figure 16, with a maximum sensitivity to  $\Delta m^2$  of  $4 \times 10^{-6} eV^2$ . The KamLAND detector should be operational in 2001.

Fig. 17. Schematic view of the KamLAND detector (from ref<sup>19</sup>)

#### 4. The $\bar{\nu}_e - d$ experiment at Bugey

Reactor neutrinos interacting with deuterons result in two reaction channels, a charged current (CC) reaction



and a neutral current (NC) reaction



As the CC reaction is sensitive to oscillations while the NC reaction is not, a measurement of the ratio of the reaction yields may serve as a test for oscillations. This scheme was first suggested by Reines et al.<sup>29</sup> and implemented at the Savannah River reactor in 1980. However, owing to incomplete understanding of the neutron efficiency for single and double neutron events, the 1980 results turned out to be unreliable. The experiment was repeated recently by Riley et al.<sup>30</sup> essentially using the same 1980 apparatus installed in the Bugey reactor in France. The detector consisted of a central cylindrical volume containing 276 kg of deuterium into which ten  $^3\text{He}$  proportional counters were immersed serving as neutron detectors. A liquid scintillator veto as well as Pb and Cd shielding surrounded the detector. In this experiment, only neutrons were counted. In addition to the reaction neutrons, however, there was a sizable number of background neutrons created by cosmic ray muons that could not be tagged with the veto.

The event rate for one-neutron events (NC) was  $37.7 \pm 2.0$  per day with a background rate of  $57.0 \pm 1.5$  per day. The rate for the two-neutron events (CC) was  $2.45 \pm 0.48$  with a background of  $3.26 \pm 0.36$  per day.

After correcting for the efficiencies for detecting one neutron and two neutrons of  $0.29 \pm 0.01$  and  $0.084 \pm 0.006$ , respectively, as determined with the help of a  $^{252}\text{Cf}$  source and model calculations, the ratio of the reaction yields for CC and NC divided by that calculated was found to be  $0.96 \pm 0.23$  consistent with 1, thus in agreement with the prediction. It appears that this result differs substantially from their 1980 work<sup>29</sup> with the same detector.

On account of the relatively large statistical errors and the close distance (18.5m) to the reactor, the experiment's sensitivity to oscillations was only modest allowing it to exclude an area in the parameter space with large mixing angles. The work also confirmed the calculated cross sections describing the neutrino-deuteron break-up in the CC and NC channels.

## 5. Neutrino Magnetic Moment

If neutrinos have mass, they may have a magnetic moment. An experimental effort to look for a neutrino magnetic moment, therefore, is of great interest. Some indications for a magnetic moment have come from a suggested correlation of the signal in the  $^{37}\text{Cl}$  experiment with solar activity, suggesting a value of  $10^{-11} - 10^{-10} \mu_{\text{Bohr}}$ . In addition, considerations of a possible resonant spin flavor precession (RSFP), and also of neutrino interactions in supernovae have been mentioned.

The neutrino magnetic moment contributes to the  $\nu_e e$  scattering<sup>31</sup> as shown in Fig. 18. This contribution is most pronounced at low electron-recoil energy. At about 300 keV the magnetic moment scattering is roughly equal to the weak scattering.

Previous results by Reines et al.<sup>32</sup> from scattering reactor neutrinos on electrons in a 16 kg plastic scintillator have given  $\mu_\nu = 2 - 4 \times 10^{-10} \mu_B$ . More recently, Gurevitch et al.<sup>33</sup>, using a 103 kg  $C_6F_6$  target found  $\mu_\nu < 2.4 \times 10^{-10} \mu_B$ , and Derbin et al.<sup>34</sup> with a 75 kg Si target found  $\mu_\nu < 1.8 \times 10^{-10} \mu_B$ . A recent analysis<sup>36</sup> of the Super-Kamiokande data<sup>35</sup> results in a limit of  $\mu_{\nu\mu} < 1.6 \times 10^{-10} \mu_B$ .

Fig. 18. Contribution of the neutrino magnetic moment to the  $\bar{\nu}_e e \rightarrow \bar{\nu}_e e$  scattering, averaged over the reactor  $\bar{\nu}_e$  spectrum. The purely weak cross section is also shown. (From Vogel and Engel<sup>12</sup>)

An effort to obtain a value or stringent limit of  $\mu_\nu$  is now underway by the MUNU experiment, a Grenoble-Munster-Neuchatel-Padova-Zurich collaboration<sup>37</sup> which has built a 1000 liter  $CF_4$  TPC at 5atm (18.5 kg), surrounded by an anti-Compton shield. This detector is now installed at the Bugey reactor in France. The expected event rate in the interval of 0.5 to 1 MeV recoil energy is 5.1 per day, at an expected background of 4.5 per day. Implementing the angular correlation of the scattered electrons with

respect to the incoming reactor neutrinos is expected to enhance the signal-to-noise significantly. A schematic view of the MUNU TPC is shown in Fig. 19.

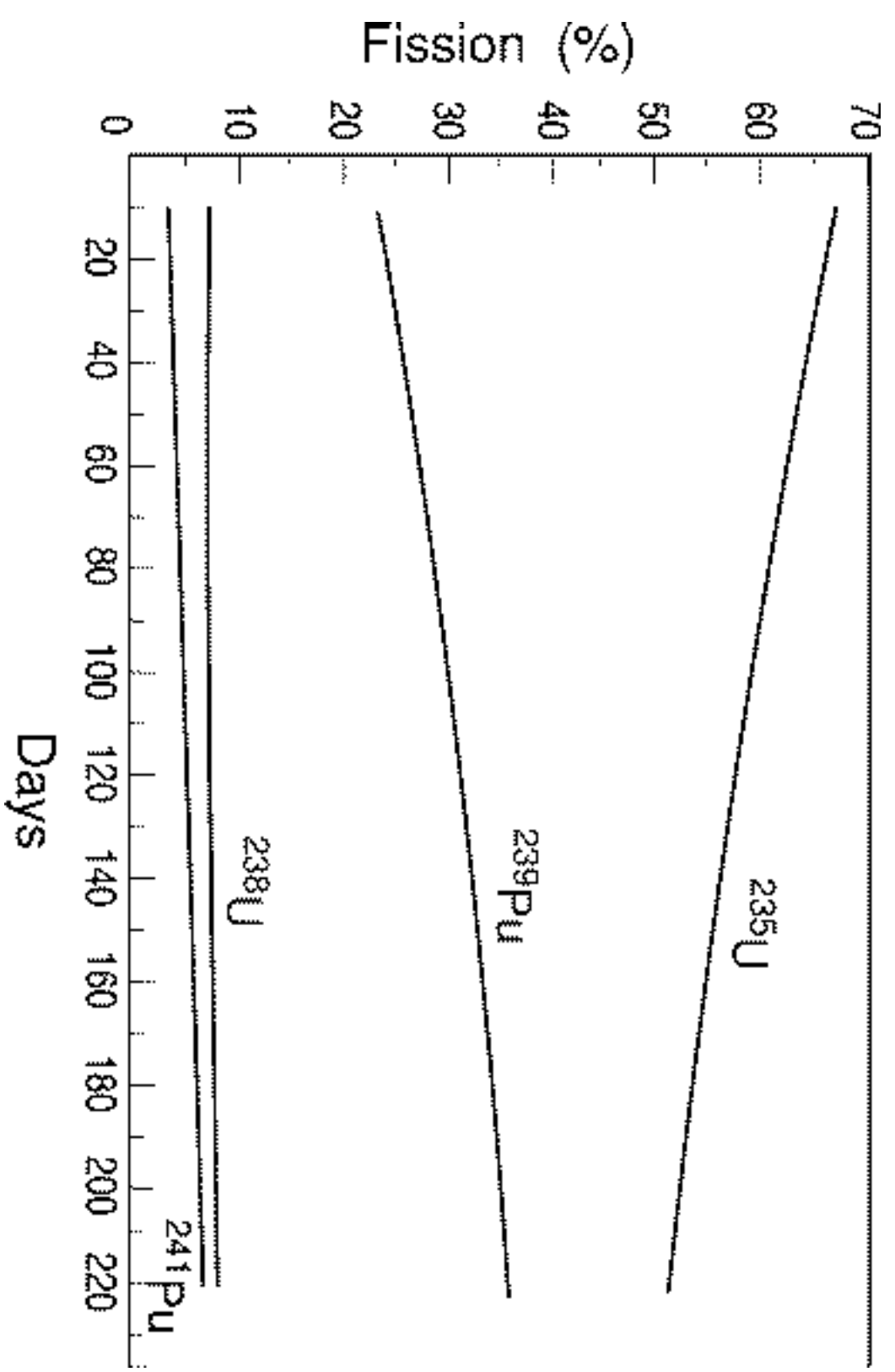
Fig. 19. Layout of the MUNU detector for the measurement of the neutrino magnetic moment.

## 6. Conclusion

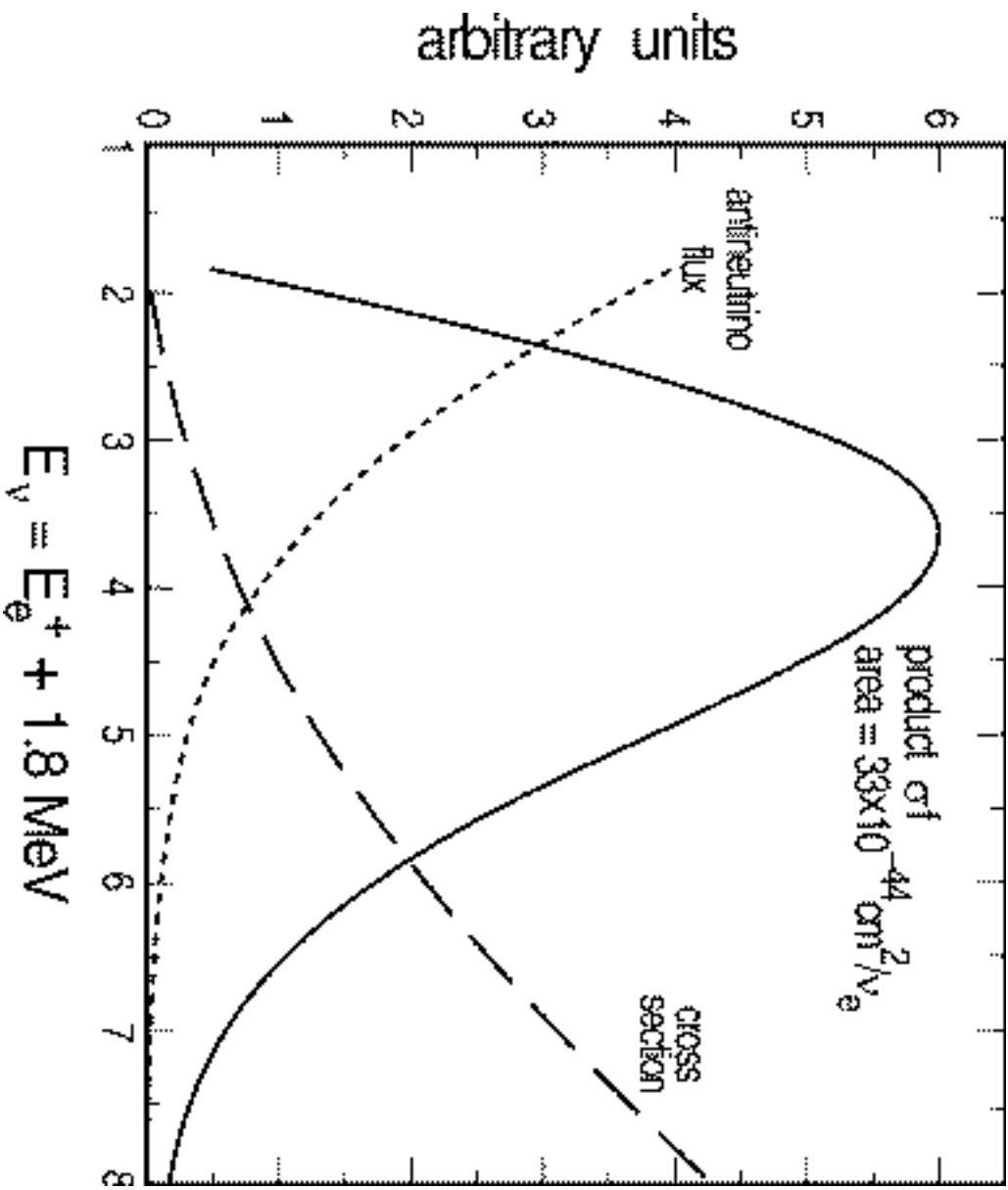
Reactor neutrinos with their low energies are well suited to explore small  $\Delta m^2$  for the  $\bar{\nu}_e$  disappearance channel. From the results of the Chooz and Palo Verde experiments it can be concluded that the atmospheric  $\nu_\mu$  deficiency cannot be attributed to  $\bar{\nu}_\mu \leftrightarrow \bar{\nu}_e$  oscillations. The Chooz experiment has ruled out this channel with large confidence level, and the first data set from Palo Verde excludes it at 90% CL. To improve on the mixing angle sensitivity in these experiments so as to shed light on a possible 3-flavor solution will be a challenging task. The KamLAND experiment at a very large baseline is now on the drawing board. Searches for a neutrino magnetic moment from the MUNU experiment are in progress.

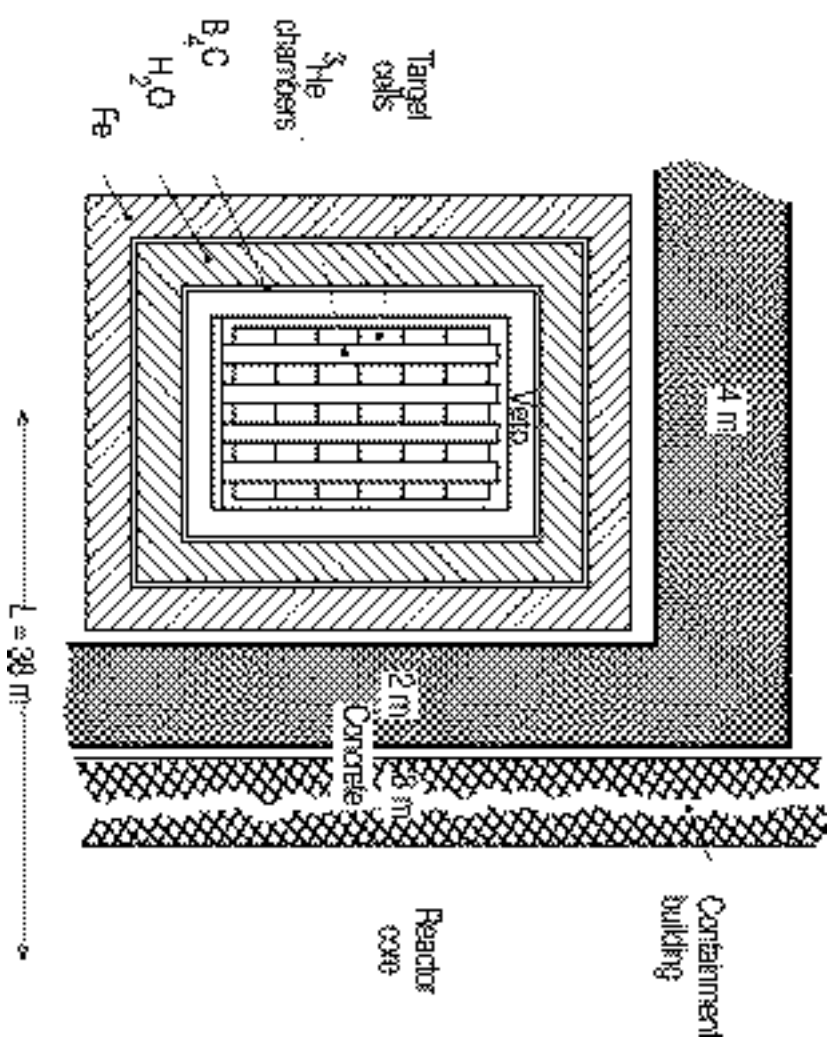
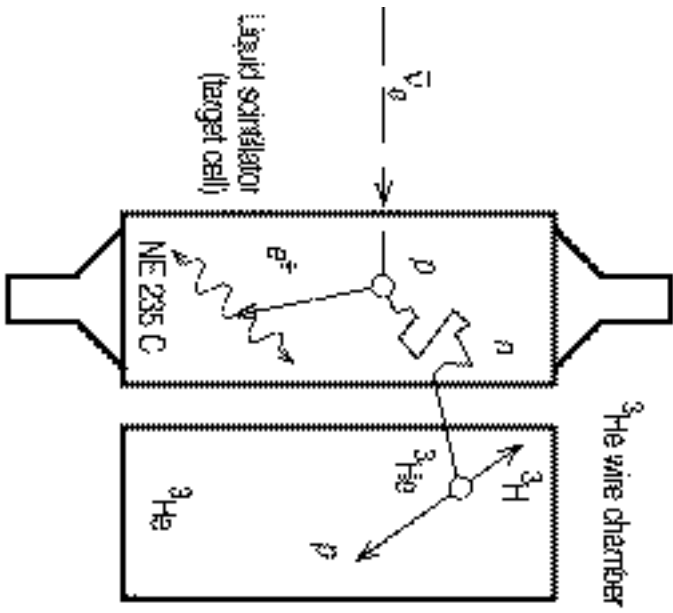
1. See, for example, F. Boehm and P. Vogel, *Physics of Massive Neutrinos*, Second Edition, Cambridge University Press (1992).
2. H. Kwon et al., *Phys. Rev. D* **24** (1981) 1097.
3. G. Zacek et al., *Phys. Rev. D* **34** (1986) 2621.
4. B. Achkar et al., *Nucl. Phys. B* **434** (1995) 503.
5. M. Apollonio et al., *Phys. Lett. B* **420** (1998) 397; M. Apollonio et al., *Phys. Lett. B* **466** (1999) 415.
6. F. Boehm et al., *Phys. Rev. Lett.*, **84** (2000) 3764, F. Boehm et al. *Phys. Rev. D*, to be published; hep-ex/0003022.
7. Y. Fukuda et al., *Phys. Lett. B* **335** (1994) 237.
8. J. N. Bahcall, P. I. Krastev and A. Y. Smirnov, *Phys. Rev. D* **58**, 096016 (1998).
9. P. Vogel et al., *Phys. Rev. C* **24** (1981) 1543.
10. K. Schreckenbach et al., *Phys. Lett. B* **218** (1989) 365.
11. Y. Declais et al., *Phys. Lett. B* **338** (1994) 383.
12. P. Vogel and J. Engel, *Phys. Rev. D* **39** (1989) 3378.
13. P. Vogel, private communication.
14. See, for example, S. M. Bilenky and P. Pontecorvo, *Physics Report* **41** (1978) 225, H. Fritzsch and P. Minkowski, *Phys. Lett. B* **62** (1976) 72.
15. A. A. Kuvshinnikov et al., *JETP Lett.* **54** (1991) 255.
16. A. I. Alfonin et al., *JETP* **67** (1998) 213.
17. G. S. Vidyakin et al., *JETP Lett.* **59** (1994) 390.
18. Y. Fukuda et al., *Phys. Rev. Lett.* **81** (1998) 1562.

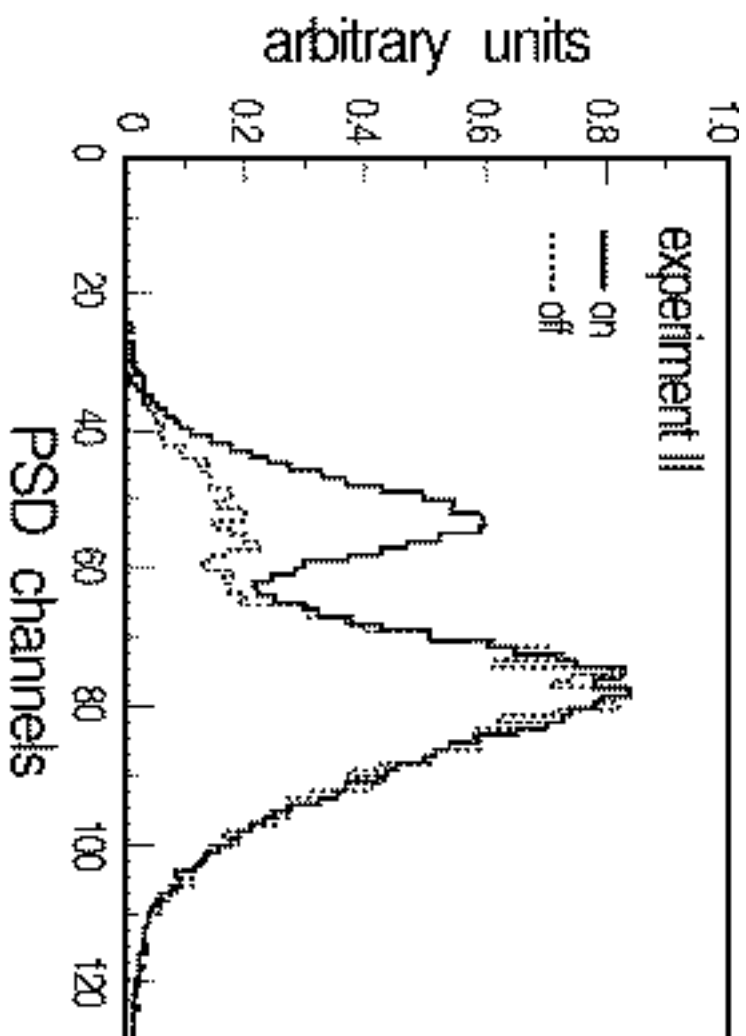
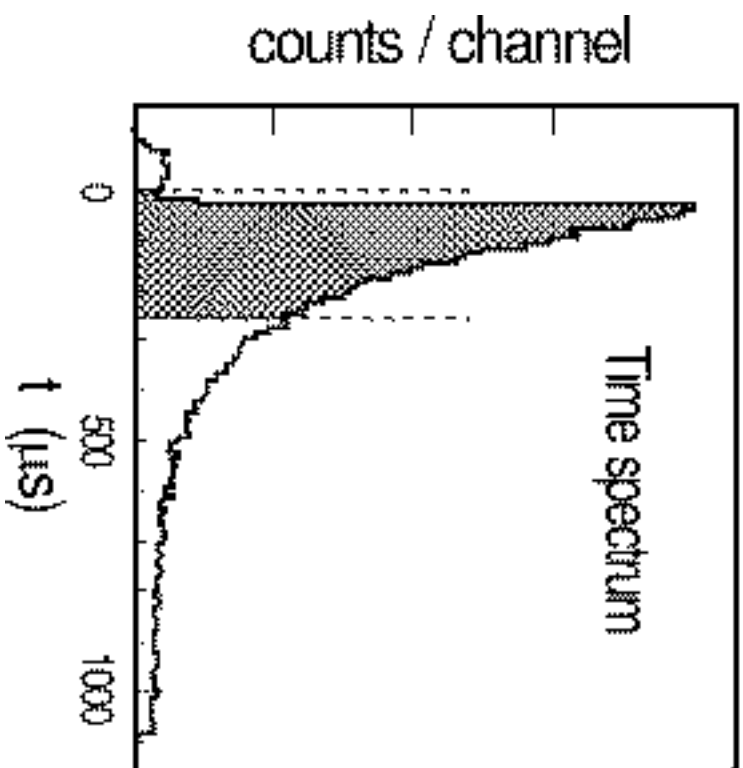
19. P. Alvisatos et al., KamLAND, a Liquid Scintillator Anti-Neutrino Detector at Kamioka, Stanford-HEP-98-03, Tohoku-RCNS-98-15 July 1998 (unpublished); A. Piepke, in *Neutrino 2000, International Conference on Neutrino Physics and Astrophysics*, Sudbury, Canada, June 16 - 21, 2000.
20. A. Piepke et al., *Nucl.Instr.Meth.A* **432** (1999) 392.
21. A. Piepke and B. Cook, *Nucl.Instr.Meth.A* **385** (1996) 85.
22. G.J. Feldman and R.D. Cousins, *Phys.Rev.D* **57** (1998) 3873.
23. Y-F. Wang, L. Miller, and G. Gratta, *Phys.Rev.D* bf 61 (July 2000) to be published; hep-ex/0002050.
24. P. Vogel and J. F. Beacom, *Phys.Rev.D* **60** (1999) 053003; K.B. Lee, private communication.
25. G. Zacek, Thesis, Technical University of Munich (1984).
26. F. Boehm, in *Eighth International Workshop on Neutrino Telescopes*, Venice, Feb 23 - 26, 1999, Ed. M. Baldo Ceolin, Edizioni Papergraf (1999).
27. K.Okumara, PhD Thesis, University of Tokyo, unpublished, and Super-Kamiokande Collaboration, preliminary results. See also second quoted Ref. 6.
28. M. Apollonio et al., *Phys.Rev.D* **61** (2000) 012001.
29. F. Reines et al., *Phys.Rev.Lett.* **45** (1980) 1307.
30. S. P. Riley et al., *Phys.Rev.C* **59** (1999) 1780.
31. P. Vogel and J. Engel, *Phys.Rev.D* **39** (1989) 3378.
32. F. Reines et al., *Phys.Rev.Lett.* **37** (1976) 315.
33. I.I. Gurevitch et al., *JETP Lett.* **49** (1989) 740.
34. A.I. Derbin et al., *JETP Lett.* **57** (1993) 768.
35. Y. Fukida et al., *Phys.Rev.Lett.* **82** (1999) 2430.
36. J. F. Beacom and P. Vogel, *Phys.Rev.Lett.* **83** (1999) 5222.
37. C. Amsler et al., *Nucl.Instr.Meth.A* **396** (1997) 115.

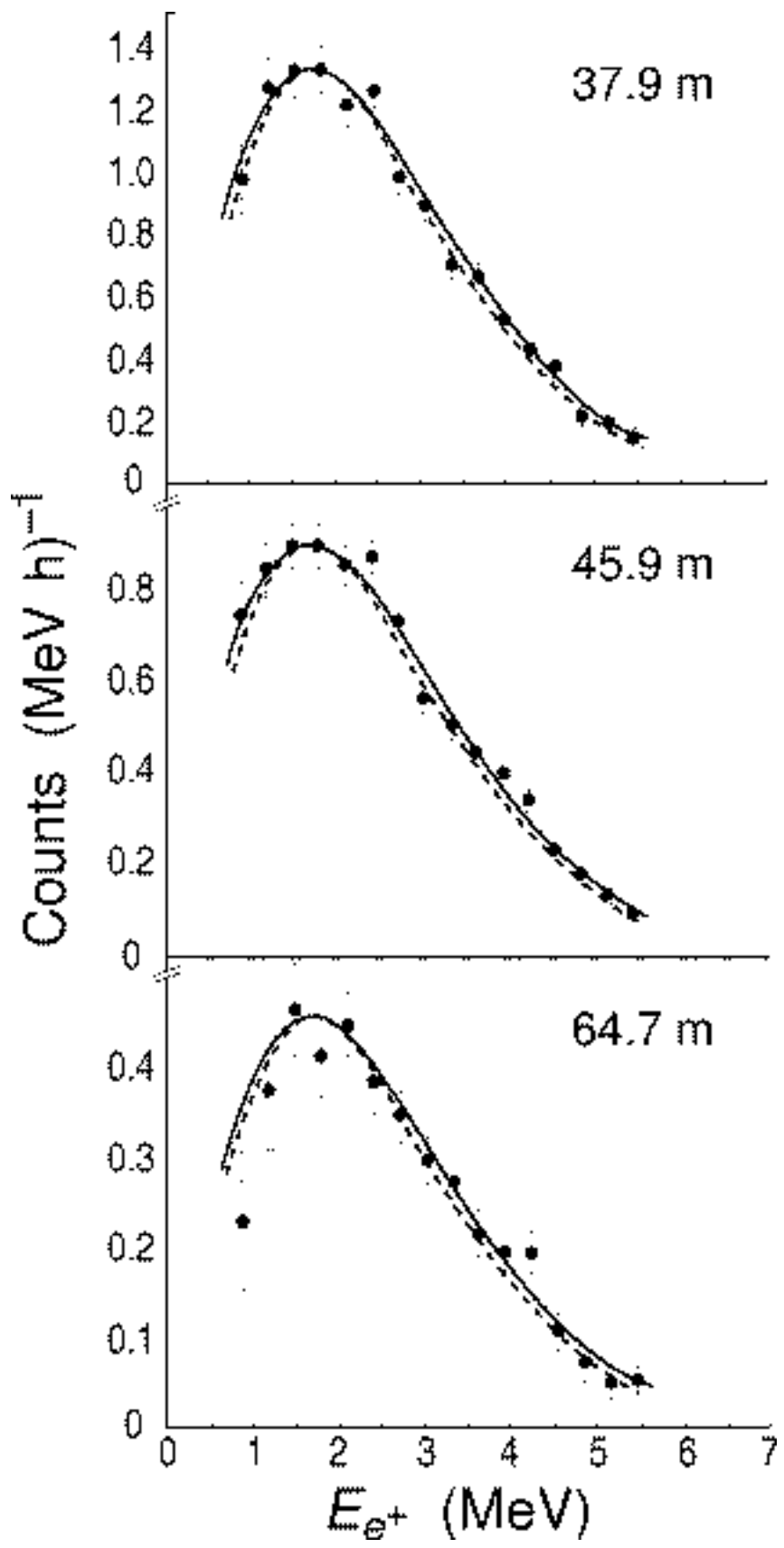


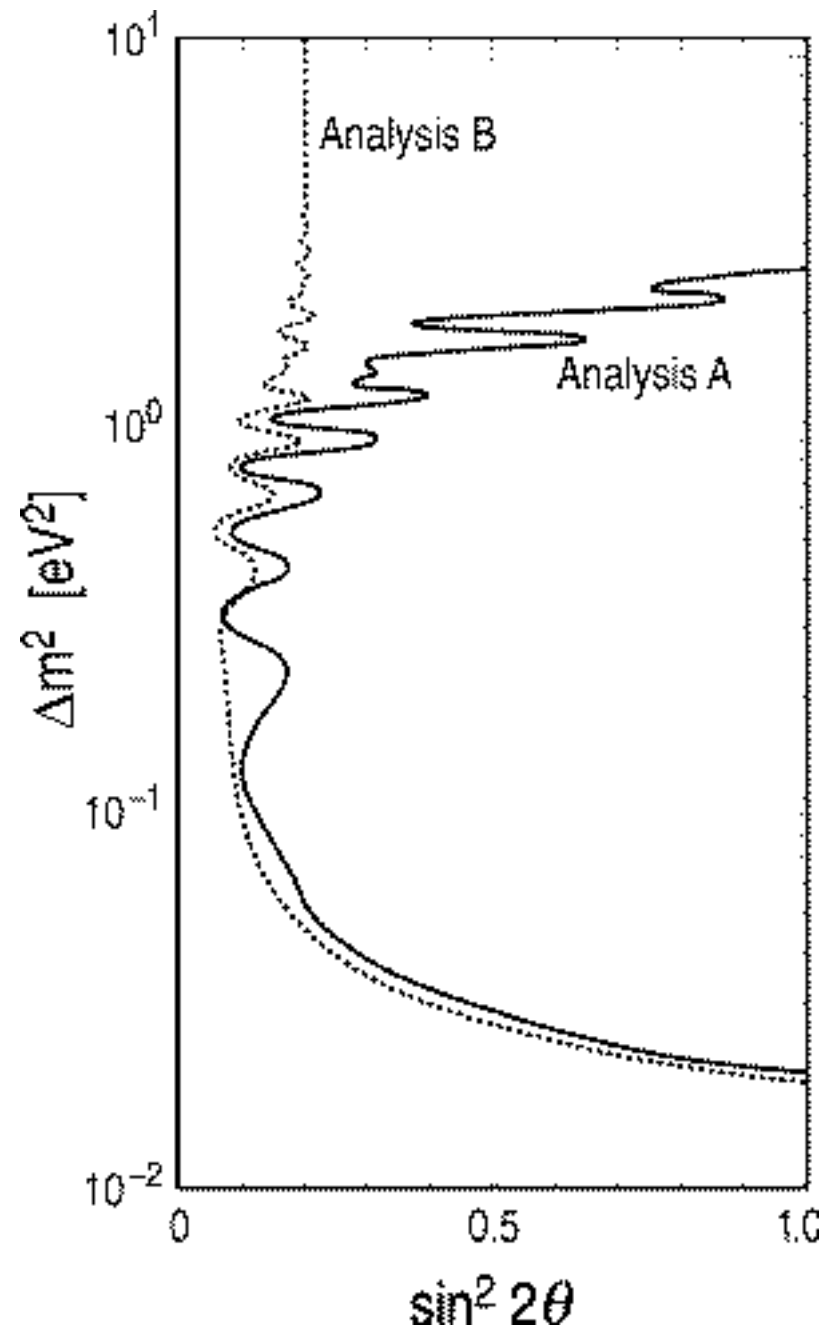




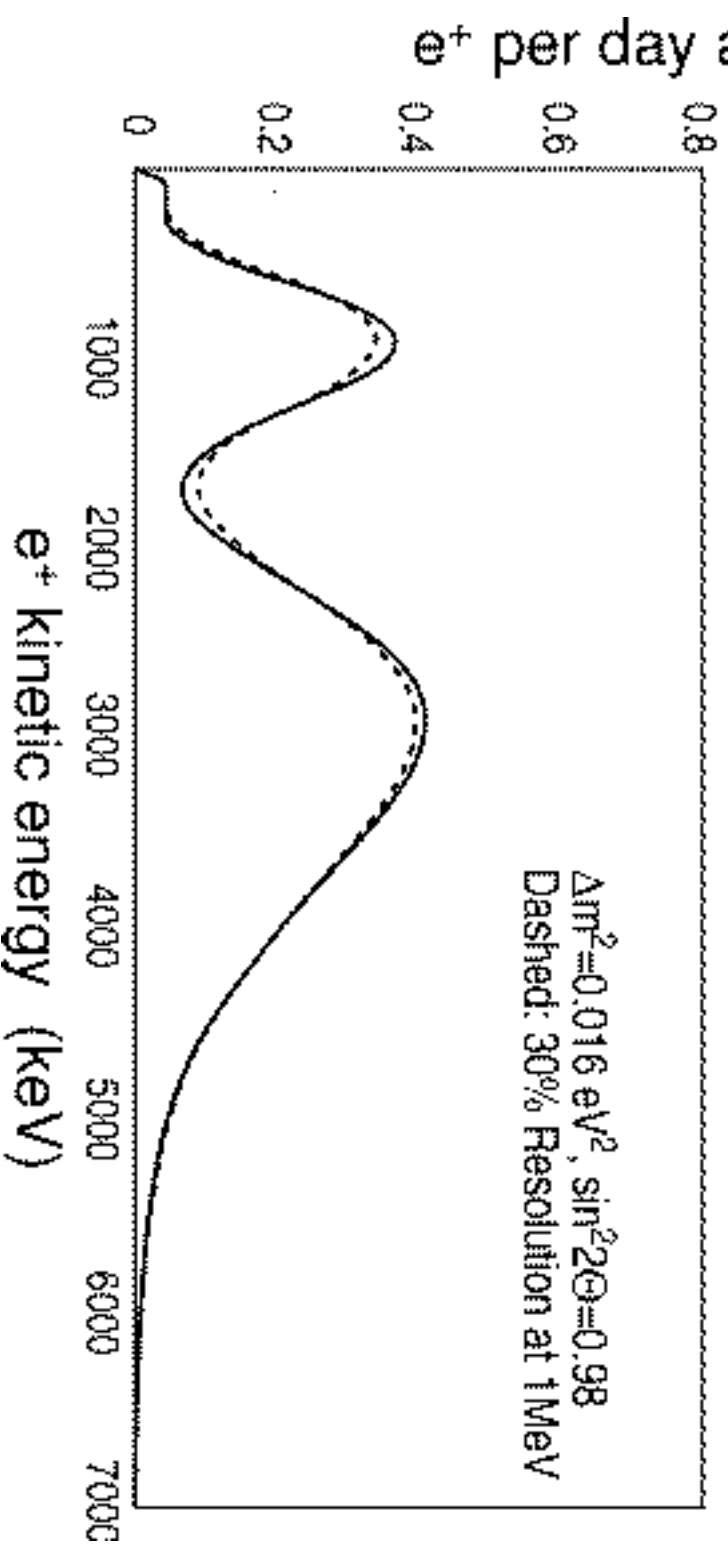
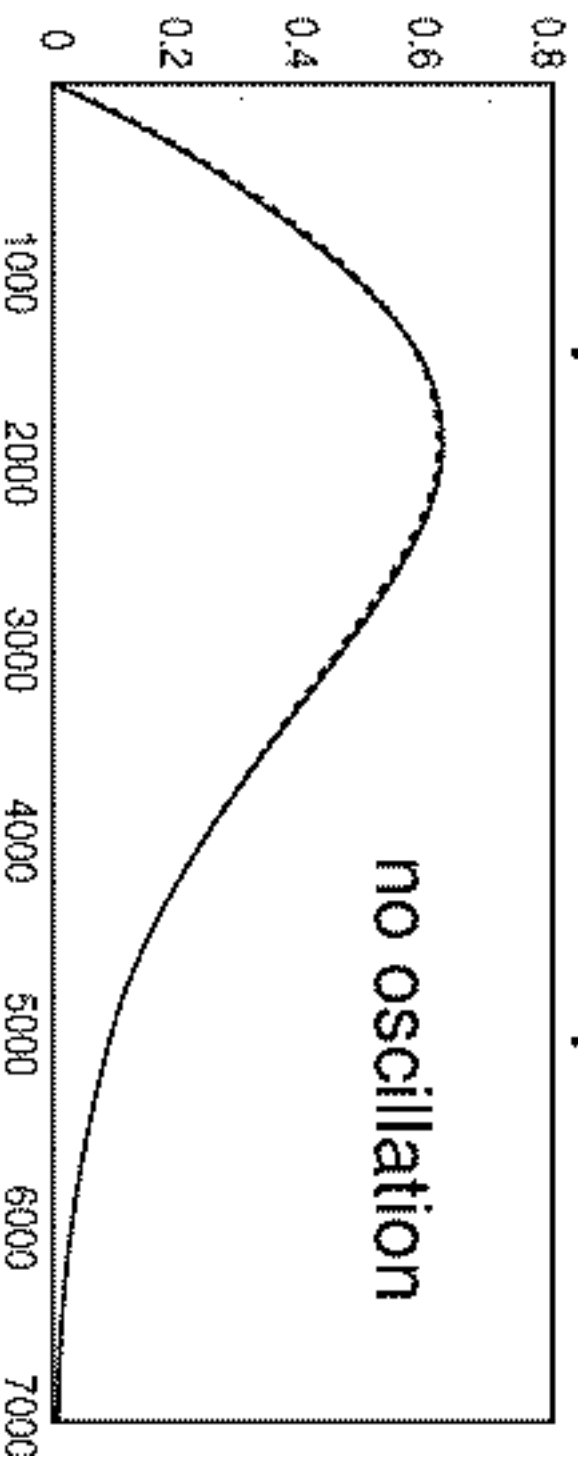


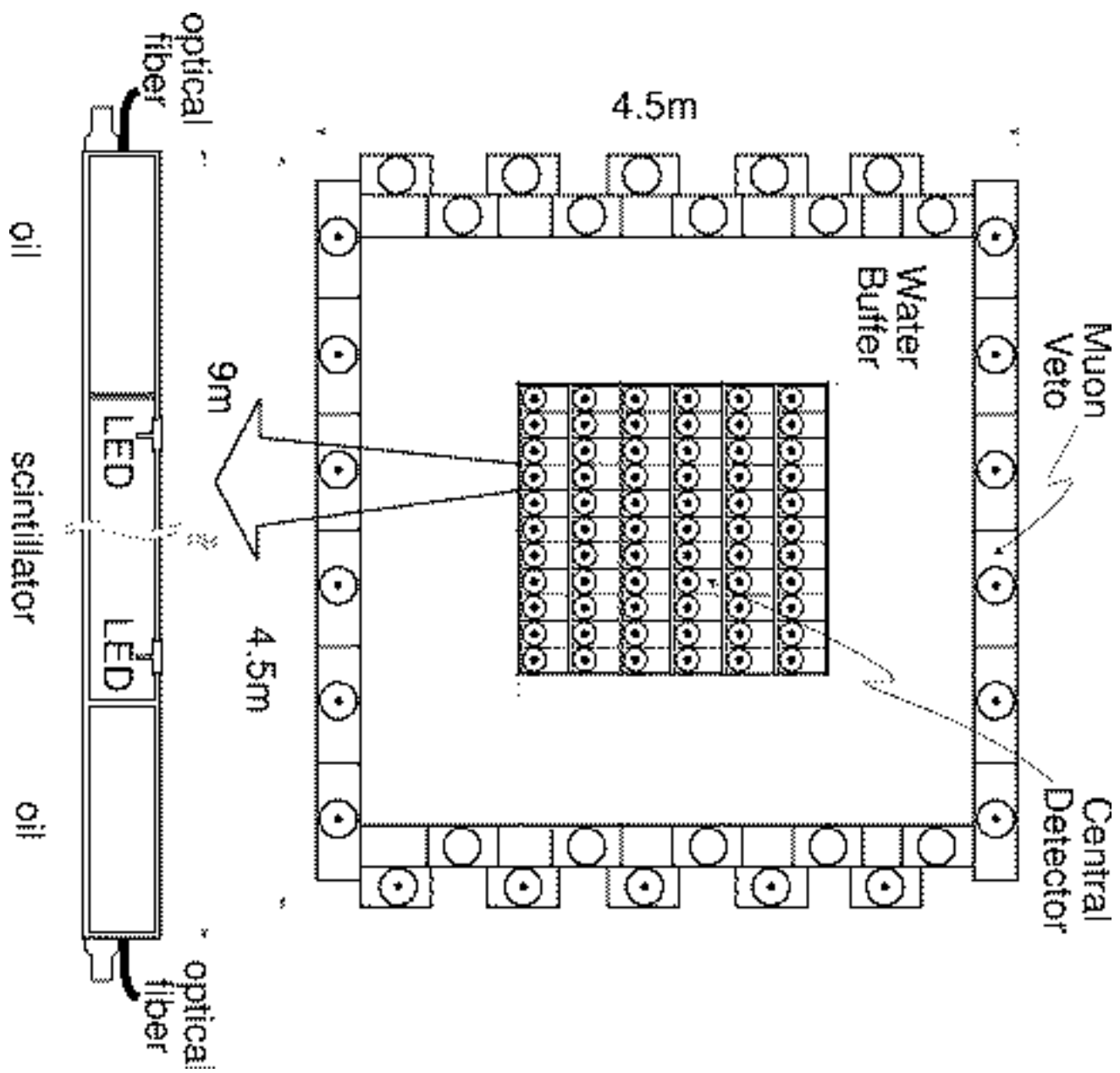




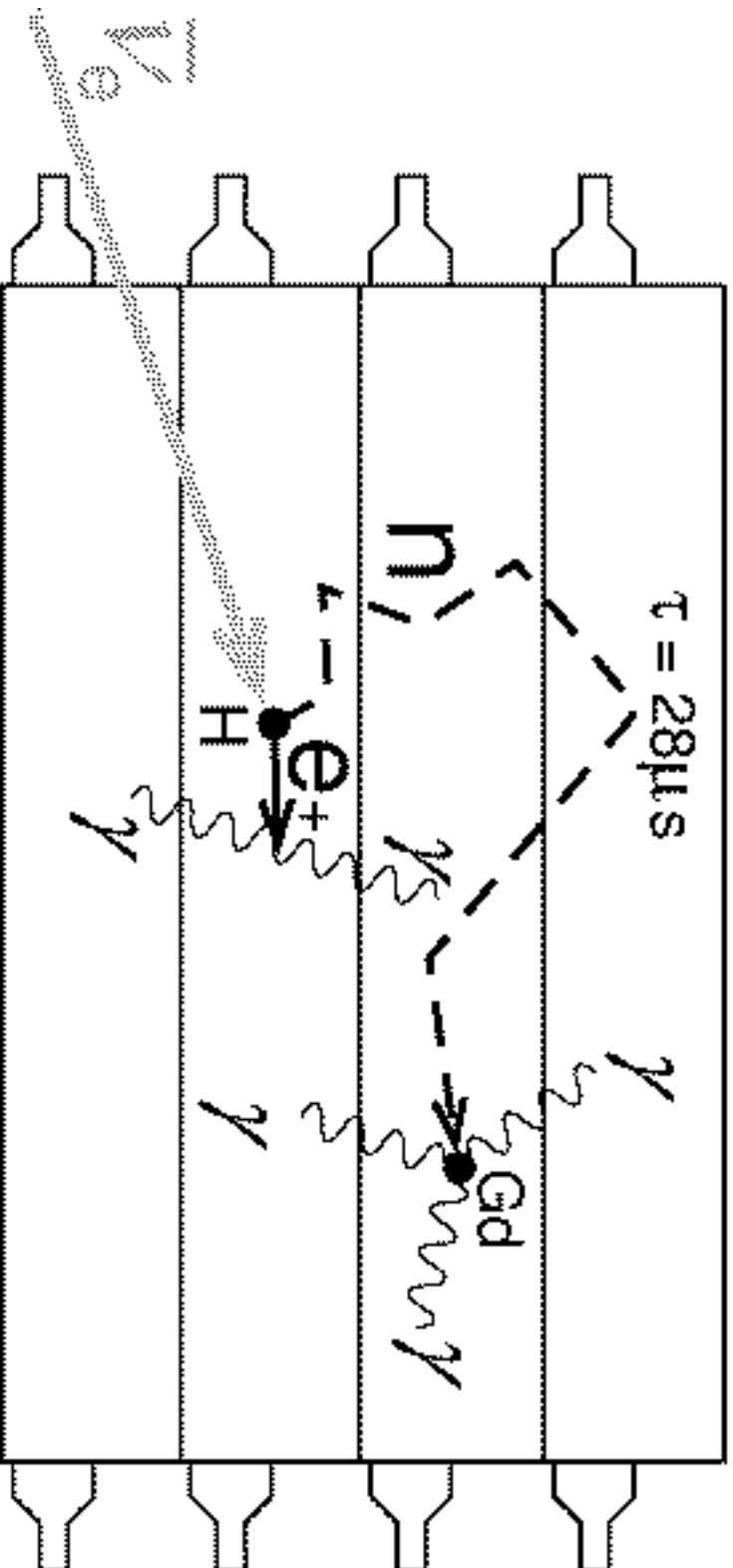


# Expected PV no-osc. spectra



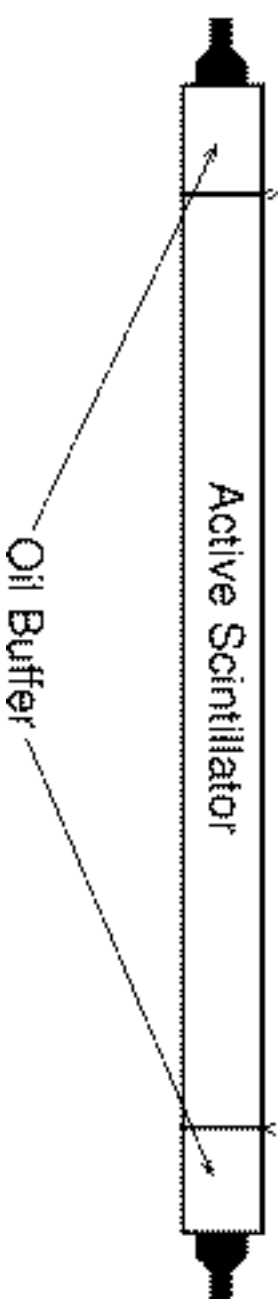
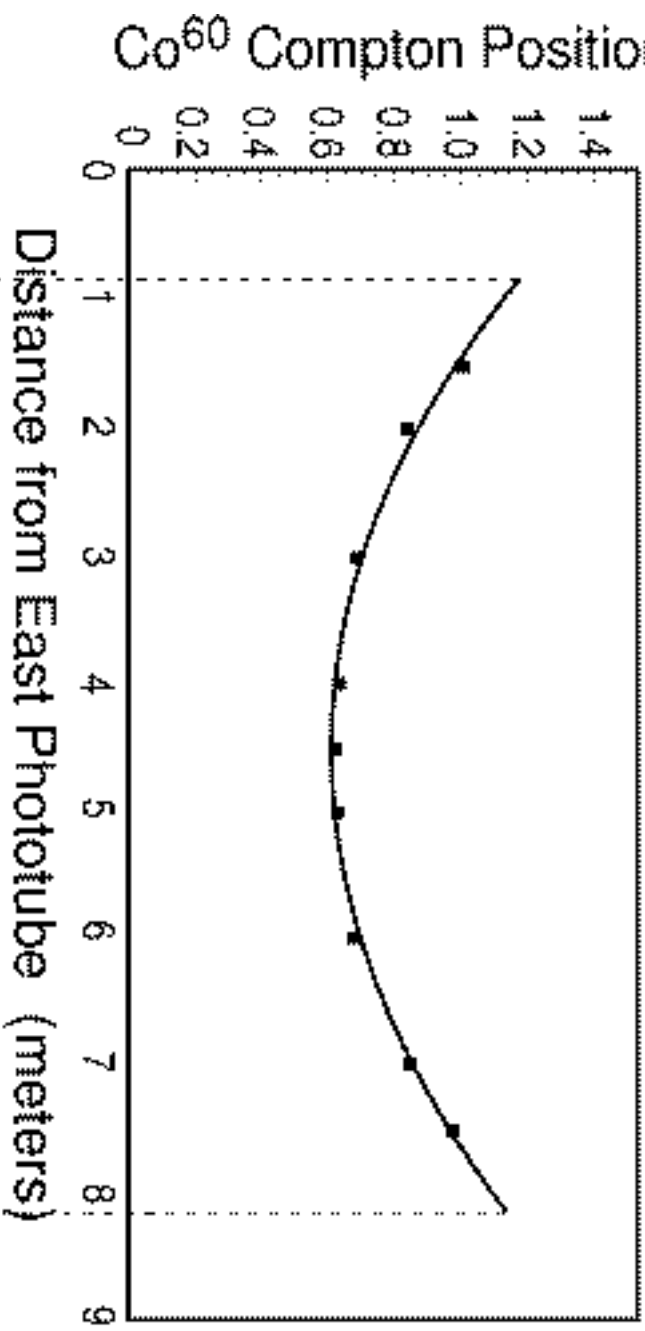


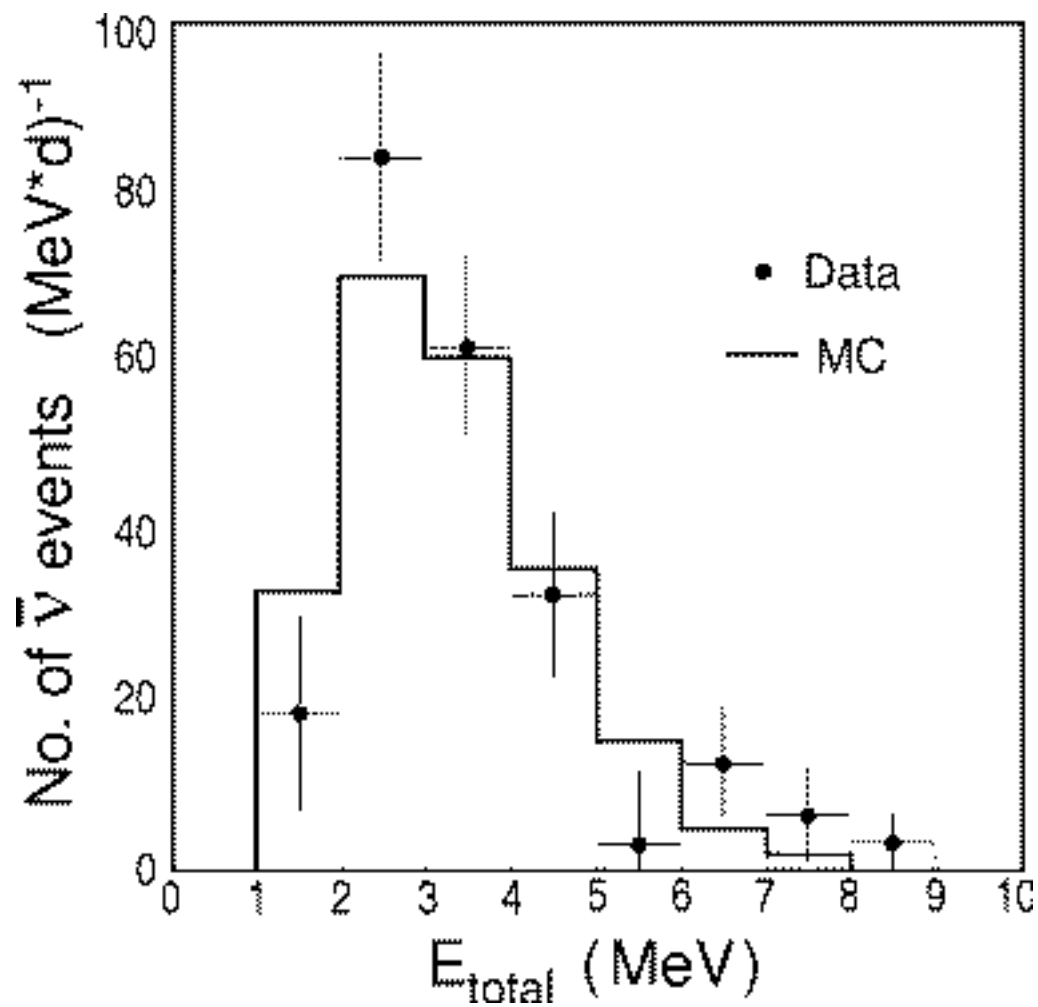
## V-reaction in PV detector matrix

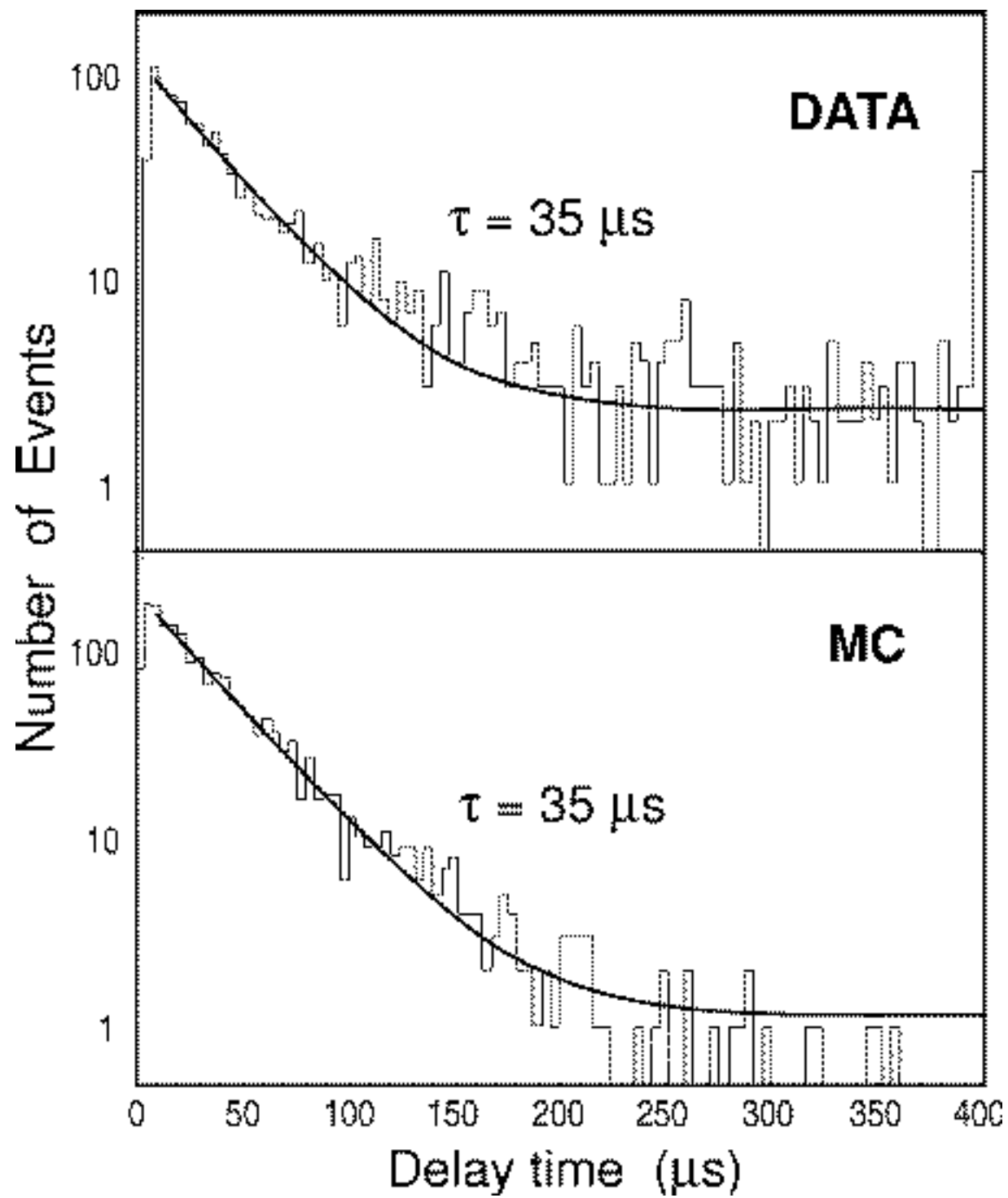


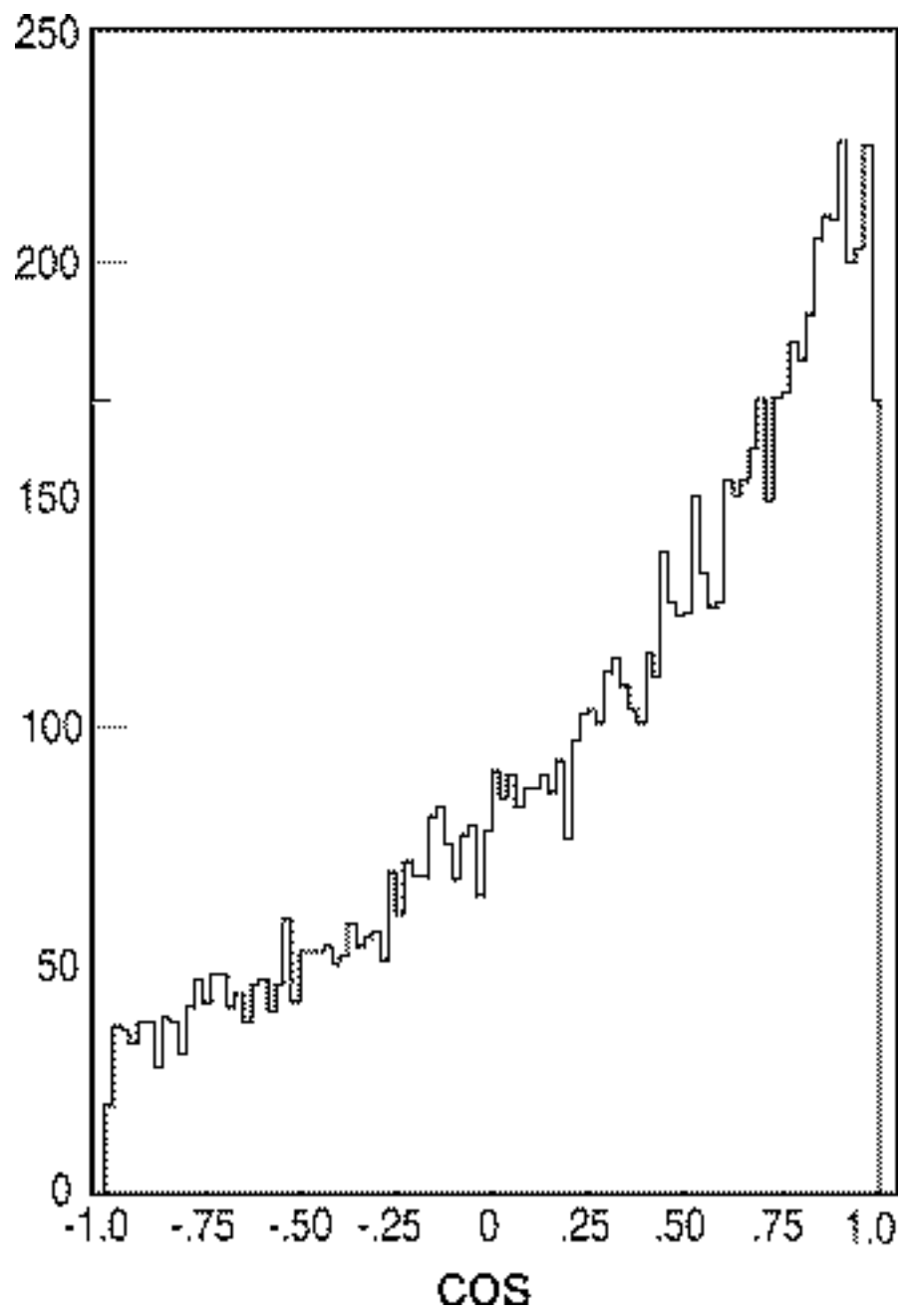


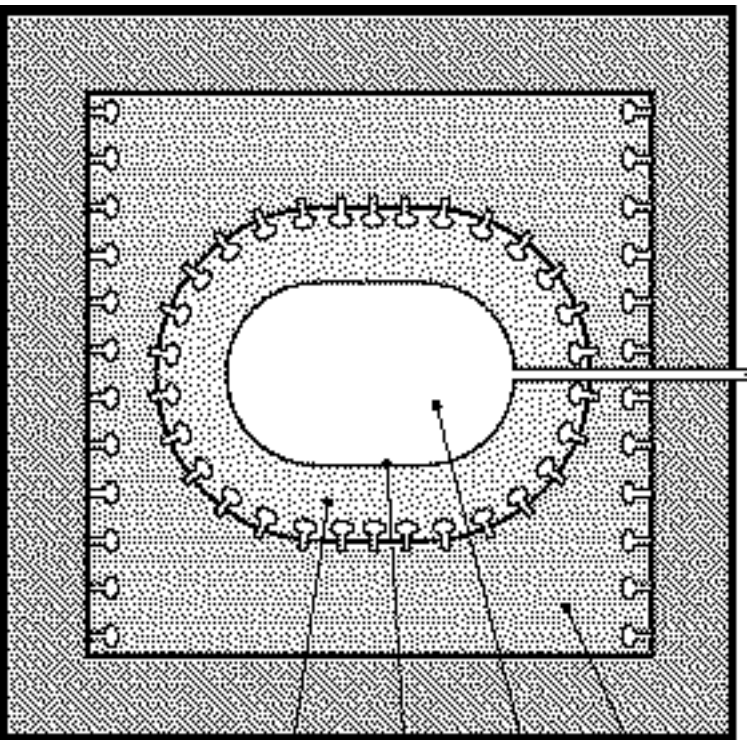
Position dependence of calibration along 9m tank











veto, 90 t

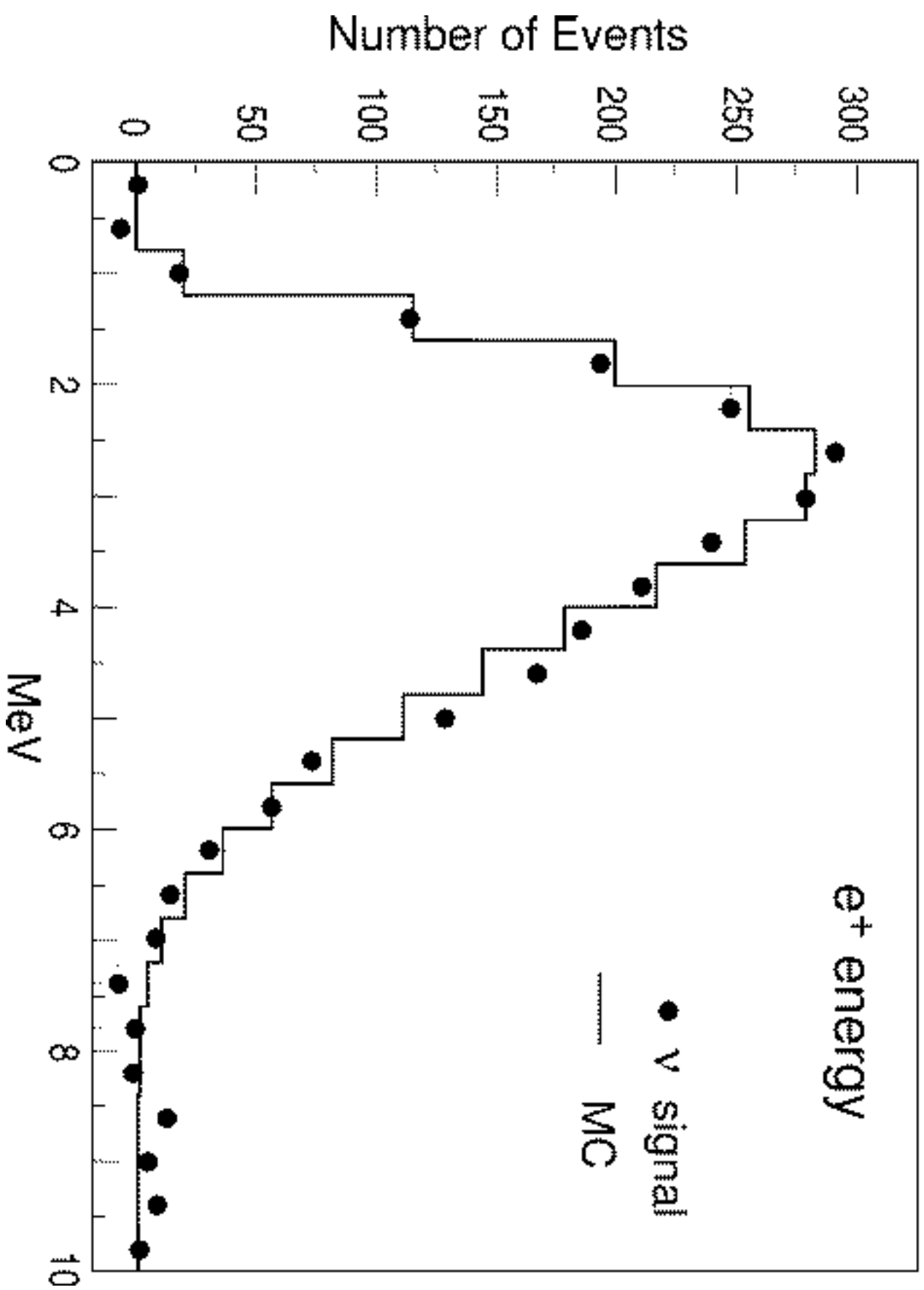
v - Target, 5 t

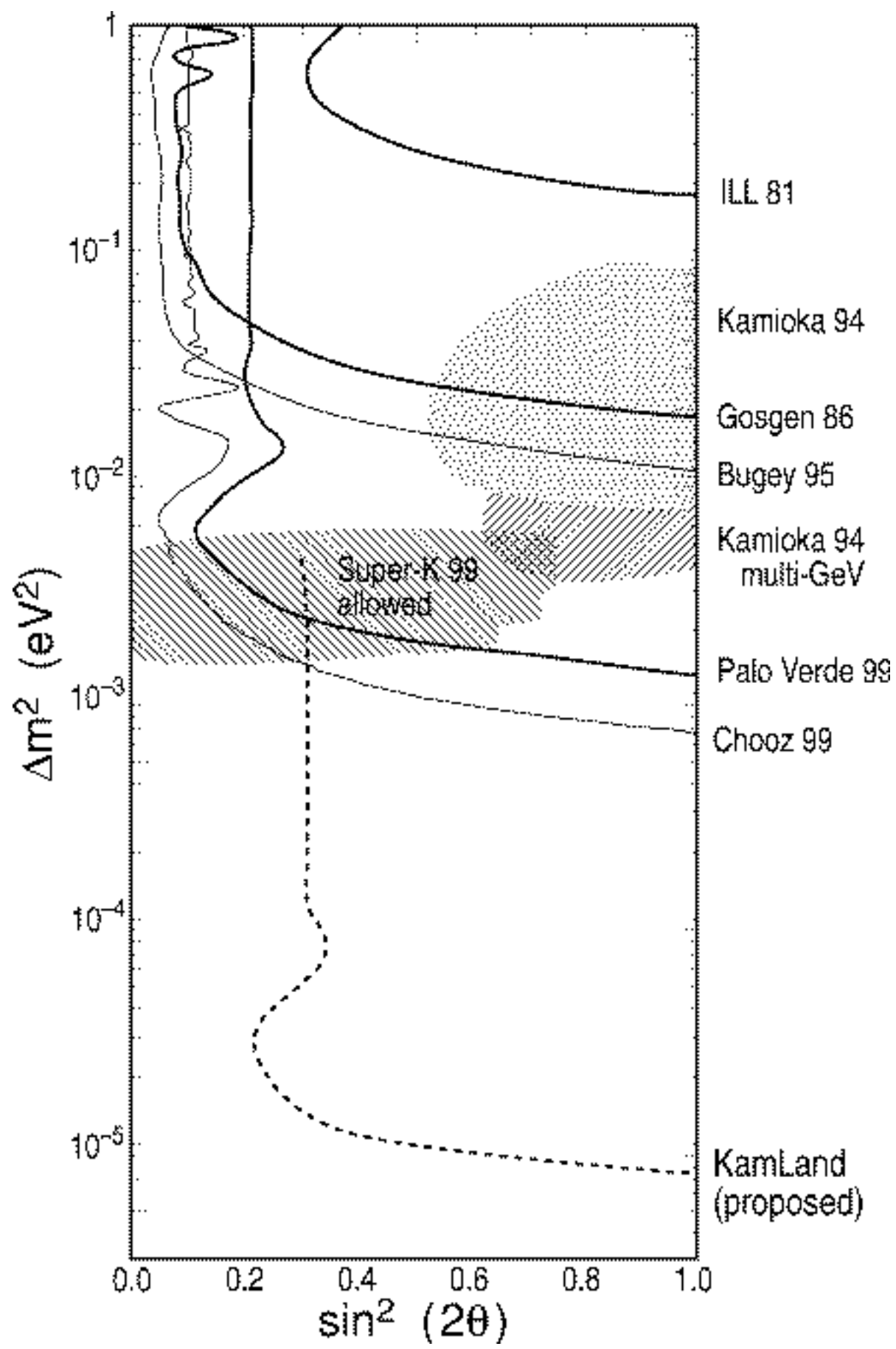
Acrylic vessel

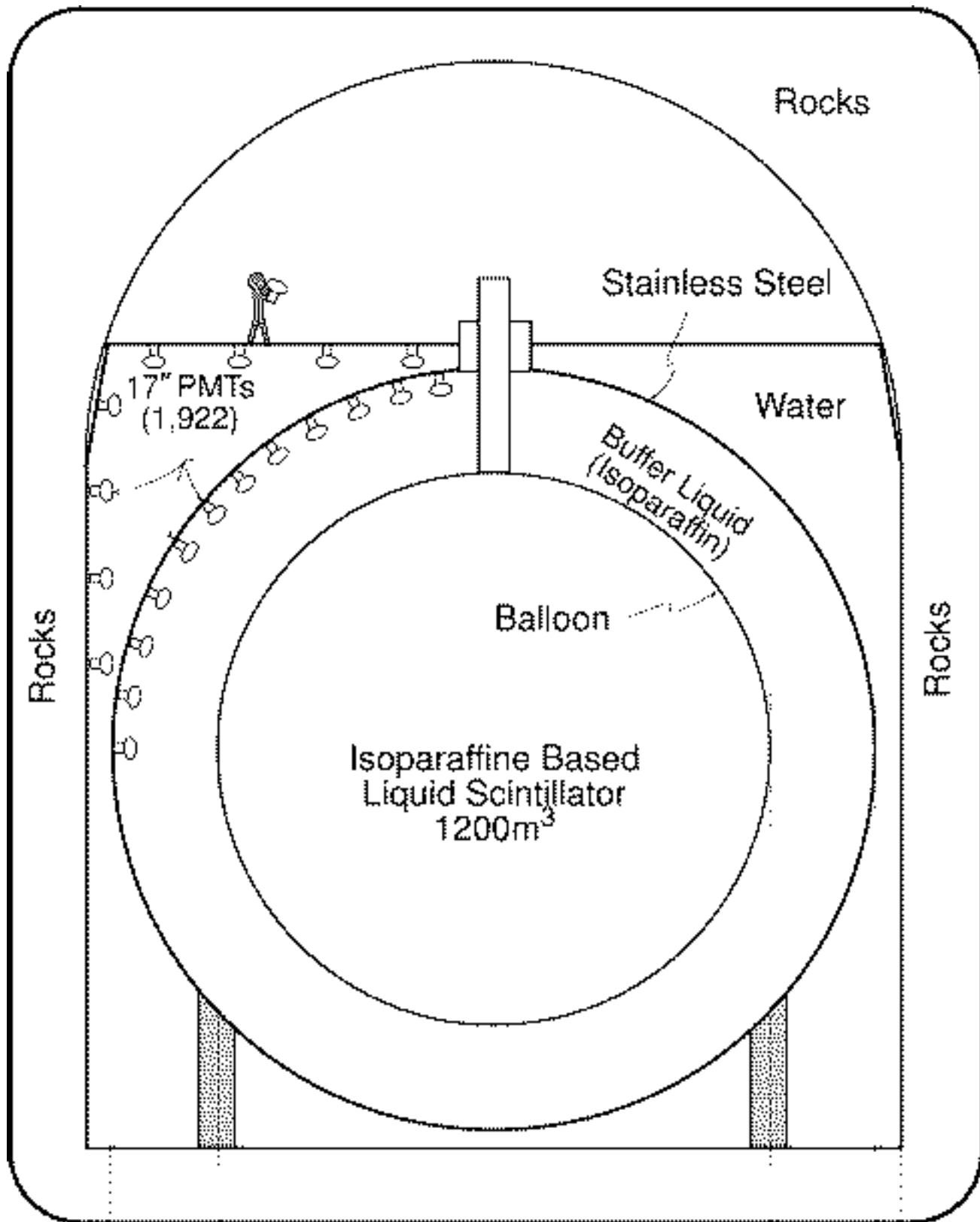
Containment region, 17 t



All Data







13 m

18 m

20 m



